

Construction of an Enzyme Cascade Based on the Accurate Adjacent Arrangement of Coupled Enzymes Using a Triblock PolyA DNA Probe

Lele Wang,[†] Ruiyan Guo,[†] Lanying Li, Qing Tao, Qin Xu, Xue Yang, Xue Liu, Jiang Li, Lihua Wang, Jinxue Chang, Chengming Cao, Yanli Wen,^{*} Shiping Song,^{*} and Gang Liu^{*}



Cite This: *JACS Au* 2024, 4, 228–236



Read Online

ACCESS |



Metrics & More



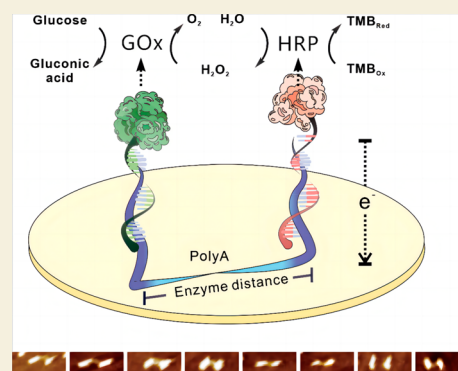
Article Recommendations



Supporting Information

ABSTRACT: Intracellular enzyme cascades are essential for various biological processes, and mimicking their functions in artificial systems has attracted significant research attention. However, achieving convenient and efficient spatial organization of enzymes on interfaces remains a critical challenge. In this work, we designed a simple single-DNA scaffold using triblock polyA single-stranded DNA for the arrangement of coupled enzymes. The scaffold was assembled onto a gold electrode through the affinity of polyA–Au, and two enzymes (glucose oxidase and horseradish peroxidase) were captured through hybridization. The molecular distance between the enzymes was regulated by changing the length of the polyA fragment. As a proof of concept, a glucose biosensor was constructed based on the enzyme cascade amplification. The biosensor exhibited excellent detection capability for glucose in human serum samples with a limit of detection of 1.6 μM . Additionally, a trienzyme cascade reaction was successfully activated, demonstrating the potential scalability of our approach for multienzyme reactions. This study provides a promising platform for the development of easy-to-operate, highly efficient, and versatile enzyme cascade systems using DNA scaffolds.

KEYWORDS: polyA, enzyme cascade, electrode, glucose



INTRODUCTION

Intracellular enzyme cascades play vital roles in biological systems,¹ enabling various complex and sophisticated biological activities such as metabolic pathways² and biological signaling processes. Drawing inspiration from the remarkable specificity and efficiency of natural enzyme cascades,³ extensive research has been conducted⁴ to mimic their functions in artificial systems.⁵ For instance, enzyme cascades⁶ have been successfully applied to develop time-saving and cost-effective drug synthesis technologies,⁷ as well as highly specific and sensitive biosensors.⁸

The reaction efficiency of biomimetic enzyme cascades heavily depends on the spatial organization of the multi-enzymes on confined artificial interfaces.⁹ Numerous strategies have been studied for the spatial regulation of enzyme couples¹⁰ addressing two main challenges in enzyme assembly.¹¹ The first challenge lies in achieving a perfect 1:1 adjacent distribution of enzyme couples on heterogeneous interfaces, which directly impacts the reaction efficiency. The second challenge involves precisely manipulating the distance between each couple of enzymes within the critical coupling length (CCL) to facilitate efficient substrate transport.

To address these challenges, nanomaterials¹² have been explored as potential frameworks for the controllability of

assembled enzyme pairs. For instance, Willner's group¹³ realized successful 2-enzyme and 3-enzyme biocatalytic cascades in metal–organic framework nanoparticles. However, challenges related to enzyme leakage and instability persist with the application of a nanomaterial-based enzyme framework.

DNA nanotechnology¹⁴ provides a powerful tool for precise space-arrangement¹⁵ due to its structure variety,¹⁶ dynamic regulation,¹⁷ biocompatibility,¹⁸ enzyme binding stability, etc. Several self-assembled DNA nanostructures, including DNA swinging arm,¹⁹ DNA nanocage,²⁰ and DNA rectangle,²¹ have been successfully constructed for the enzyme arrangement. In this field, DNA nanostructures²² work as promising scaffolds for enzyme organizing on the nanoscale based on their programmable self-assembly.²³

To simplify the enzyme arrangement process²⁴ on interfaces, researchers have focused on developing convenient and cost-

Received: October 31, 2023

Revised: November 20, 2023

Accepted: November 28, 2023

Published: December 19, 2023



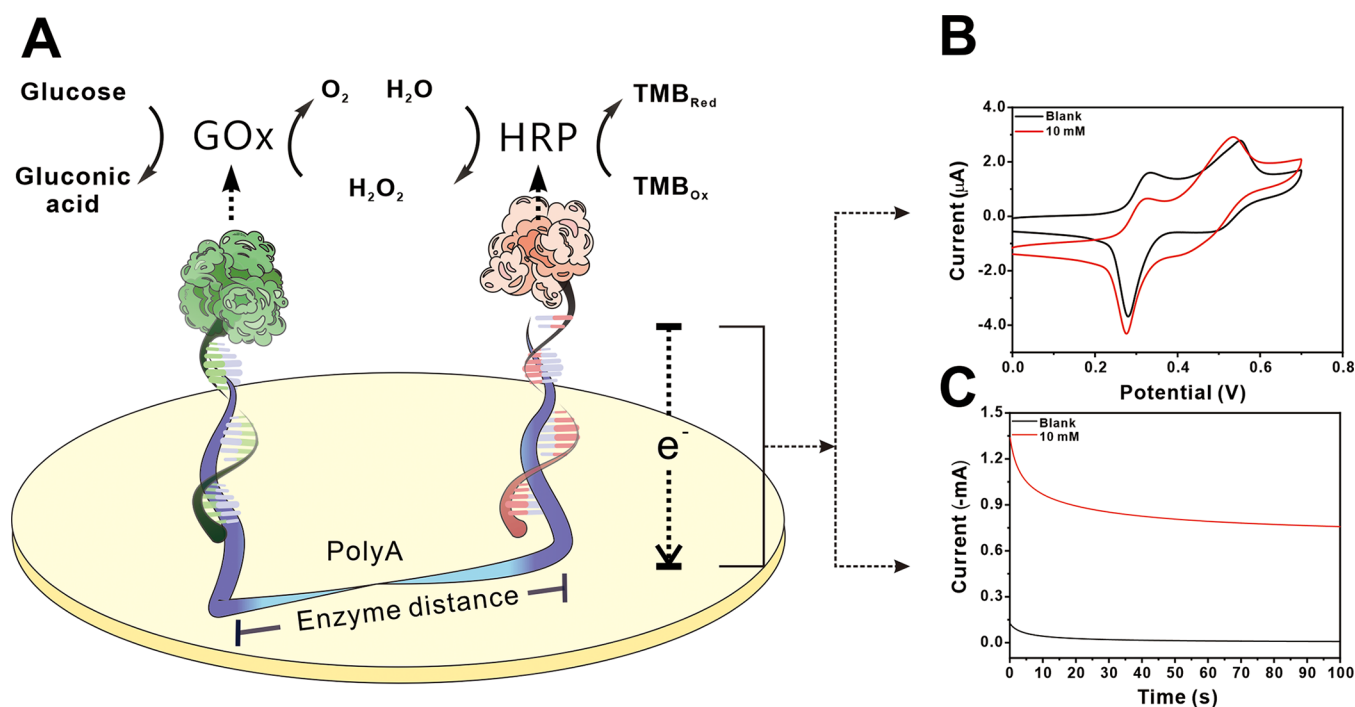


Figure 1. (A) Schematic illustration of the enzyme cascade-based electrochemical glucose biosensor and electrochemical analysis results in the absence and presence of 10 mM glucose. (B) CV circles, scan rate = 50 mV/s. (C) $I-t$ curves, potential = 100 mV.

effective solutions using fewer DNA strands. For instance, spatially addressable rectangular DNA origami contains 227 DNA strands, and a DNA tweezer consists of 9 DNA strands to precisely regulate the distance between two enzymes. Most recently, Zuo's group realized multienzyme catalytic cascade on an electrochemical interface using tetrahedral DNA framework with 4 DNA strands. However, it is still imperative to develop more easy-operating and low-cost strategies for ultimately practical engineering of multienzyme systems.

In this work, we developed a straightforward method for the arrangement of coupled enzymes on the interface. To achieve this, we utilized a triblock single-stranded DNA (ssDNA) containing a central polyA fragment flanked by two capture probes, resulting in a probe-polyA-probe (PAP)²⁵ structure. The PAP scaffold was assembled onto a gold electrode through polyA-Au affinity. By employing DNA hybridization, we were able to synchronously capture two enzymes, namely, glucose oxidase (GOx) and horseradish peroxidase (HRP). Interestingly, the molecular distance was accurately regulated by conveniently changing the length of the polyA fragment. As a proof of concept, a glucose biosensor was constructed based on the efficient enzyme cascade amplification.

RESULTS AND DISCUSSION

Construction of the Enzyme Cascade on a Triblock Probe

Two DNA-enzyme complexes were prepared by connecting two linker DNA strands with the enzyme molecules (GOx-L1 and HRP-L2). The successful formation of the DNA-enzymes was confirmed through PAGE gel analysis (Figure S1) and UV spectroscopy (Figure S2). Subsequently, a triblock probe consisting of a central polyA fragment and two flanking probes (PAP) was self-assembled onto the electrode surface by using covalent binding between adenines and Au. Once the PAP-covered electrode was prepared, the two DNA-enzymes were introduced and anchored at opposing ends of the polyA probe

through hybridization. This arrangement facilitated the formation of highly efficient one-to-one enzyme cascades (GOx and HRP) at the interface.

In our experiment, the polyA block on the PAP served multiple purposes. It not only exhibited high affinity for the electrode surface, enabling the construction of a stable and well-structured self-assembling layer (SAM), but also allowed for accurate manipulation of the molecular distance between the two enzymes by conveniently adjusting the length of the polyA segment (Figure 1A).

An enzyme-cascade reaction was initiated between two enzymes with the addition of glucose as the trigger molecule. The glucose was catalyzed by GOx, resulting in the formation of hydrogen peroxide. H_2O_2 then served as the oxidizing agent for the subsequent HRP catalysis. 3,3',5,5'-Tetramethylbenzidine (TMB) was used as the substrate of HRP and also acted as the electron-transfer mediator on the electrode, generating a detectable electrochemical catalysis signal. Cyclic voltammetry (CV) and amperometry ($I-t$) were used to investigate the electrochemical behavior of the enzyme-cascade reaction. As depicted in Figure 1B, the CV results revealed two pairs of well-defined redox peaks. Notably, upon the addition of 10 mM glucose (red line in Figure 1B), a significant increase in the peak signal at approximately 300 mV was observed. The quantitative amperometry results (Figure 1C) further supported this finding, showing that the current value for 10 mM glucose was nearly 100 times higher than that for the blank. These results demonstrate the low background and high signal-to-noise ratio (S/N) characteristic of the PAP-based electrochemical enzyme-cascade reaction.

Precise Regulation of the Molecular Distance Using the PAP

Precisely regulating the molecular distance between a pair of enzymes is crucial for subsequent enzyme cascade reactions and their biological applications, such as biosensing and

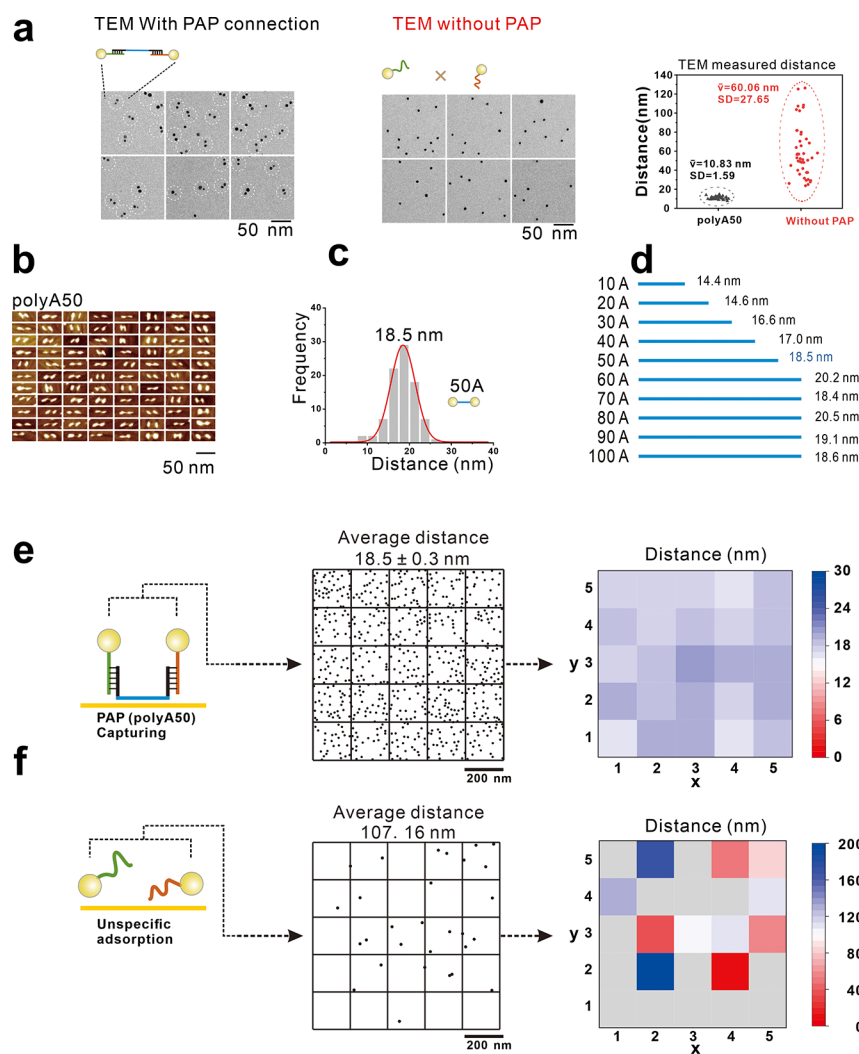


Figure 2. (a) TEM image of PolyA50-directed assembly of AuNPs on gold surface and a control result without PAP. (b) AFM images of AuNP pairs. (c) The measurements of the distance between AuNPs, (d) The distance measured using different length of polyA (polyA10 to polyA100), (e) Using a representative region of 1000×1000 nm, we divided it into a 5×5 matrix to measure the interparticle distance. The heatmap provided an overview of the average interparticle distance for each square (200×200 nm) within the matrix. Overall, the average interparticle distance for the entire area was found to be 18.5 ± 0.3 nm. (f) A control experiment without PAP. The AuNPs were added onto a bare gold surface and measured by AFM. The length of polyA is 50 nt in the PAP used in this section.

bioengineering. In this study, we developed a polyA-modified self-assembled monolayer (PAP SAM) to improve the arrangement of enzymes. The polyA block, consisting of a specific number of adenines, provided both reliable affinity to the electrode surface and controllable molecular distance by occupying the corresponding surface space between enzymes. By utilizing PAP, we achieved a precise yet easy-to-operate SAM that enabled accurate one-to-one neighborhood capture and high control over the molecule distance.

To evaluate the capability of the distance arrangement, two 6 nm diameter gold nanoparticles (AuNP-L1 and AuNP-L2) were combined with PAP through DNA hybridization. These nanoparticles served as visible labels for the two enzymes. Transmission electron microscopy (TEM) was used to examine the dispersibility and distribution of the specifically combined AuNPs on the surface. As shown in Figure 2a, TEM results of polyA50 exhibited predominantly paired dispersion of the AuNPs. Conversely, without the connection of PAP, the AuNPs were randomly distributed on the surface. TEM measured distance between the AuNPs is 10.83 nm when

connected by polyA50, and the control without PAP connection was about 60 nm. Compared with AFM results, the TEM result was small, mainly due to the different sampling of TEM. Atomic Force Microscope (AFM) imaging was then employed to study the arrangement of the AuNPs. As depicted in Figure 2b, clear pairing of AuNPs was observed, and notably, DNA strands were detected between the AuNPs in several AFM images. The AFM measurement of the distance between AuNPs (Figure 2c) provided valuable reference data for the surface arrangement of the enzymes, considering that both were realized on the PAP covered gold interface. Supporting Information (Figure S3–S13) showcased further TEM and AFM results of PAP using different length (polyA10–100). Figure 2d illustrates that the distance between AuNPs increased as polyA fragments extended from 10 to 50 nt, eventually reaching a plateau beyond 50 nt. Consequently, polyA50 was selected as the optimal length of the PAP for subsequent experiments. However, as a flexible single-strand DNA, the capability of space arrangement of PAP was limited below 50 A (polyA50 = about 18 nm); when the length of

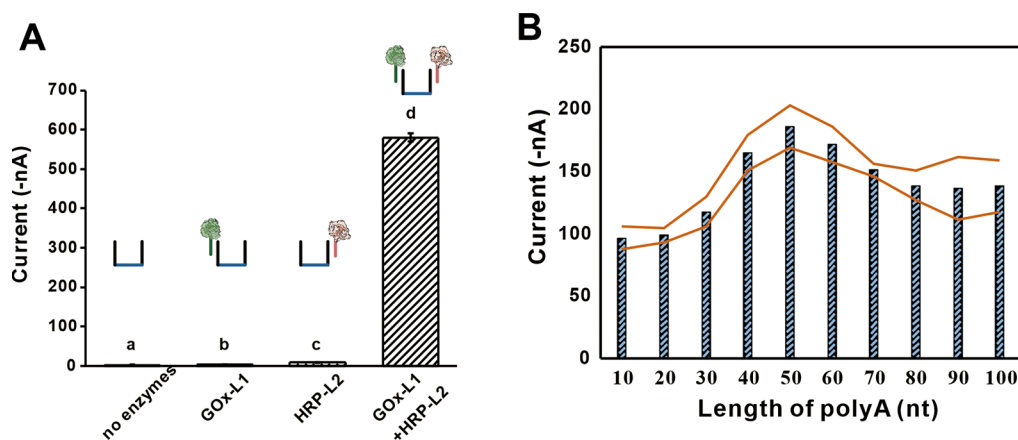


Figure 3. (A) Comparison of the electrochemical signals using different enzymes hybridized onto our PAP: (a) no enzyme, (b) GOx-L1 individually, (c) HRP-L2 individually, or (d) GOx-L1 and HRP-L2. (B) Current signal from the enzyme cascade reaction using different lengths of the polyA fragment in the PAP system. The two red lines represent the error bars of the columns.

polyA was further extended beyond 60 nt, the distance remained about 20 nm, and the configuration of DNA on interface may lead to vibration of the distance in AFM results as shown in Figure 2b. Fortunately, we successfully achieved spatial arrangement within the range of 10 to 20 nm, which has been commonly reported as the experimental dimension of enzyme-cascade reactions.

By comparing the large field view of AFM, it can be observed that in the presence of polyA, AuNPs exhibited predominately pairing (Figure 2e and Figure S14a). However, in the absence of polyA, the AuNP pairs were rare (Figure 2f and Figure S14b) on the gold surface. These results further demonstrated PAP's capability of molecular arrangement.

Verification of Enzyme Cascade Reaction

The enzyme cascade reaction on the electrode was studied by combining two enzymes (GOx-L1 and HRP-L2) onto two ends of the PAP through hybridization. As expected, upon the addition of glucose as a reaction trigger, the current signal exhibited a significant increase in the presence of a commercial TMB substrate. Control experiments were performed to demonstrate the construction of the enzyme cascade. First, a negligible blank signal was observed without any enzymes being combined on the electrode. Subsequently, single-enzyme electrodes (GOx-L1 or HRP-L2) were prepared by combining only one enzyme onto the PAP-covered electrode. However, none of the single-enzyme electrodes exhibited a detectable current signal compared to the blank condition (Figure 3A).

To optimize the GOx/HRP enzyme cascade reaction, we investigated the effect of varying the length of polyA fragments on the PAP probes and evaluated the resulting current signal. Remarkably, we found a close relationship between the catalytic efficiency and the spacing of the enzymes. As the results showed in Figure 3B, the current signal increased as the polyA fragments were extended, and the polyA50 exhibited the highest catalytic signal among all different probes from polyA10 to polyA100. Notably, the current signal slightly diminished when the length of polyA exceeded 60 nt. This finding aligns well with the AFM measurement (Figure 2d and Figure S15), which indicated that 60 nt served as the threshold for achieving controllable molecular spacing. Hence, we selected 50 nucleotides (nt) as the optimized length of polyA in this experiment. We believe the polyA fragment influences the final enzyme cascade signal through various

factors, including gold electrode affinity, probe surface density, and most importantly, the spacing between two enzyme molecules.

Different assembly probes were also compared. First, we applied two SH-DNA probes instead of the PAP and conducted the enzyme cascade reaction between GOx or HRP. The signal-to-noise (S/N) was found to be approximately 1/4 of our PAP based biosensor (Figure S16A). Subsequently, we employed two polyA-probes, each containing a single polyA fragment, as comparison to the PAP for glucose analysis under the same experimental conditions. The amperometric result (Figure S16B) demonstrated a decrease of approximately 50% compared to our three-block PAP-electrode. This observation suggests that approximately half of the enzymes did not effectively participate in the cascade reaction due to the absence of a precise spacing arrangement. In this case, the two enzyme molecules were randomly distributed on the surface without the necessary regulation for achieving one-to-one spacing.

Optimization of the Experimental Condition

Several critical experimental parameters were optimized to achieve optimal performance of the PAP-based enzyme cascade biosensor. First, the concentration of the PAP for self-assembling was found to affect the amount and density of capture probes on the gold electrode surface. Through comparisons ranging from 0.1 μM to 5 μM , a concentration of 1.0 μM was determined as optimal (Figure S17A).

Second, the total amount of the enzyme pair (GOx-L1 and HRP-L2) was optimized to be 0.05 nM (Figure S17B). More importantly, their molecular ratio was fine-tuned to achieve balanced cohybridization at both ends of the PAP, considering their distinct chemistry, dimensions, and DNA-enzyme hybridization efficiency. As the results showed (Figure S17C), the highest signal-gain was achieved using a molar ratio of 10:1 (GOx-L1: HRP-L2) between 0.2:1 to 20:1. Additionally, we studied the addition of 6-Mercapto-1-hexanol (MCH) after PAP assembling, and finally proved that an optimized concentration of 0.1 mM was ideal (Figure S17D). This concentration of MCH was capable of blocking the unspecific adsorption and keeping the PAP upright for the subsequent hybridization; however, an excessive amount of MCH may replace the PAP on the electrode surface.

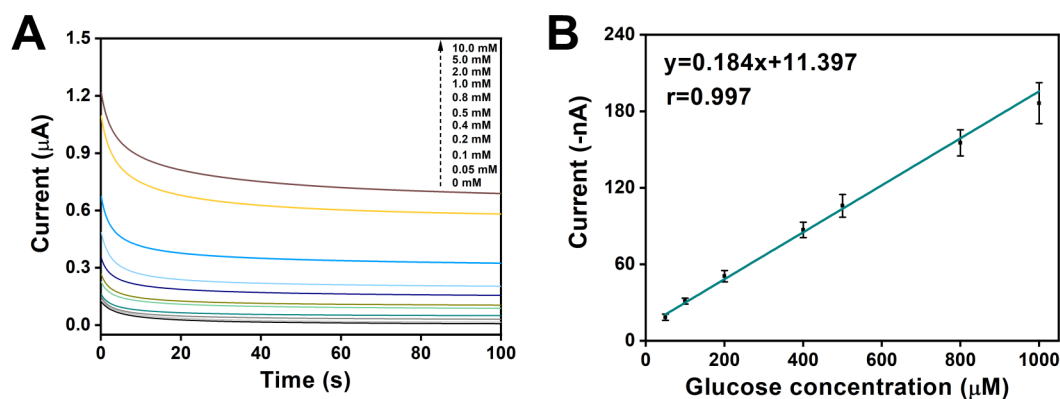


Figure 4. (A) The *I*-*t* curves of our biosensor in the presence of different concentration of glucose (bottom to top: 0, 0.05, 0.1, 0.2, 0.4, 0.5, 0.8, 1.0, 2.0, 5.0, and 10.0 mM). (B) Calibration plot showing current plotted against glucose concentration ranging from 0.05 to 1.0 mM.

The amount of N-succinimidyl 3-(2-pyridyldithio)-propionate (SPDP) used for the conjugation of the DNA-enzyme played a crucial role in both the efficiency of conjugation and the catalytic activity of the final product. As Figure S18 shows, the highest electrochemical signal was observed when the enzyme-to-SPDP ratio reached 1:10 for the conjugation of both GOx and HRP. Consequently, the enzyme-to-SPDP ratio of 1:10 was selected for DNA-enzyme conjugation.

Performance for the Enzyme Cascade-Based Biosensor

We conducted a systematic investigation into the detection performance of our enzyme-cascade-based biosensor with glucose as the target analyte. Figure 4A shows the *I*-*t* curve, indicating an increase in amperometric current as the concentration of glucose rises from 50 μM to 10 mM. Furthermore, we obtained a strong linear relationship between the amperometric current response and glucose concentration (Figure 4B). The linear regression equation was determined as $y = 0.184x + 11.397$, with a high correlation coefficient of 0.997. The corresponding detection limit (LOD) was found to be 1.6 μM (3σ). When compared to previously reported methods for the glucose assay (Table 1), our strategy

Table 1. Comparison of the Proposed Biosensor with Other Reported Works for Glucose Detection

Analytical method	Detection limit (μM)	Linear range (mM)
Colorimetric ²⁶	3.2	0–0.02
Colorimetric ²⁷	15	0.02–0.67
Fluorescent ²⁸	5.4	0.01–0.1
Fluorescent ²⁹	0.8	0.002–0.17
Electrochemiluminescent ³⁰	3.3	0.01–0.2
Electrochemical ³¹	17	0.05–0.7
Electrochemical ³²	1.86	0.01–2
Electrochemical (this work)	1.6	0.05–1

demonstrated a wider linear range and a lower LOD, which can be attributed to the utilization of a highly effective enzyme cascade reaction within the enzyme cascade system.

We evaluated the practicality of the sensor by detecting glucose in real samples. Human serum was spiked with three different concentrations of glucose (5, 12, and 20 mM final concentration) and analyzed using our biosensor. The quantification results and the corresponding recovery were listed in Table 2. As the results showed, the practicability was strongly demonstrated, because the recovery results were all close to 100% with a relative standard deviation (RSD) below

Table 2. Recoveries of Glucose in Human Serum Samples (N = 3)

Sample	Added (mM)	Detected (mM)	Recovery (%)
1	5	5.09 ± 0.25	101.8
2	12	11.88 ± 0.45	99.0
3	20	20.40 ± 0.77	102.0

5.0%. To further validate the accuracy of our sensor, we analyzed these samples by ID LC-MS/MS and ID GC-MS. Figure 5A illustrates the excellent agreement between the results obtained from our PAP-based biosensor and those from ID LC-MS/MS and ID GC-MS for the three different levels of glucose, confirming the reliability and accuracy of our sensor. Additional detailed information can be found in Figures S19 and S20.

Additionally, we evaluated the specificity of the proposed biosensor by analyzing five similar sugars (galactose, fructose, sucrose, xylose, and mannose) using the same condition. Figure 5B clearly demonstrates that, in comparison to glucose, all the nonspecific sugars generated minimal signals even at concentrations two times higher than that of glucose. These findings provide compelling evidence of the exceptional specificity of our glucose biosensor.

Generalizability of our PAP System for Enzyme Cascade

An important advantage of our polyA-based cascade system is its potential scalability to multienzyme reaction by conveniently using multiblock polyA probes.

When more enzyme molecules are captured onto the same probe, more complex multienzyme cascade reaction can be performed. To demonstrate the generalizability of our polyA-based enzyme cascade on electrochemical interface, we constructed a trienzyme cascade reaction, by designing a 5-block probe (PAPAP, probe1-polyA-probe2-polyA-probe3). Similar to the two-enzyme system, the amyloglucosidase (AM)-DNA combined with the probe and catalyzed the hydrolysis of amylos, producing glucose as the initiator of the following GOx/HRP enzyme reactions. Just as Figure 6 shows, when amylos was added onto the trienzyme electrode, the cascade reaction of AM/GOx/HRP was successfully activated. As a reliable comparison, a blank sample without amylos produced only a negligibly weak current signal.

CONCLUSIONS

Biomimetic enzyme cascades have been attracting considerable amounts of research energy in various fields; however, the

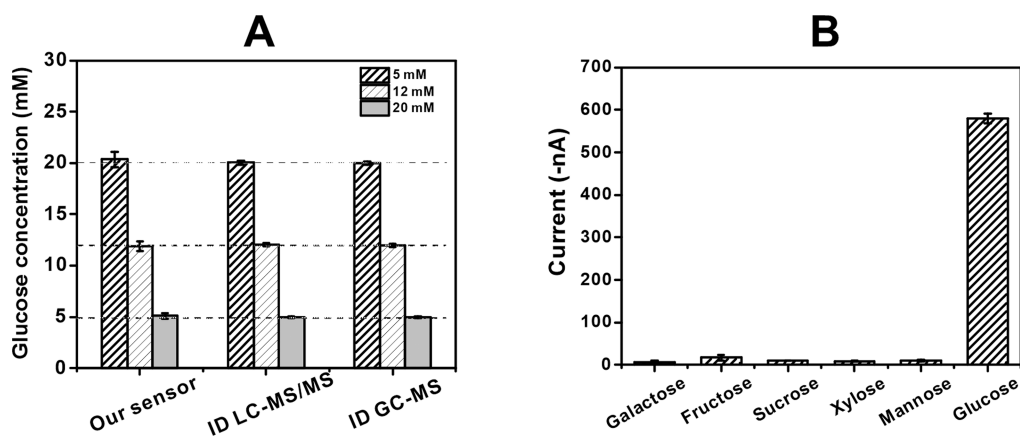


Figure 5. (A) A comparison of glucose quantification results in human serum samples using our sensor, ID LC-MS/MS, and ID GC-MS. (B) A selectivity test for glucose detection, where the glucose concentration was 5 mM while the other sugars were at 10 mM. The error bars represent the standard deviation of three repeated measurements.

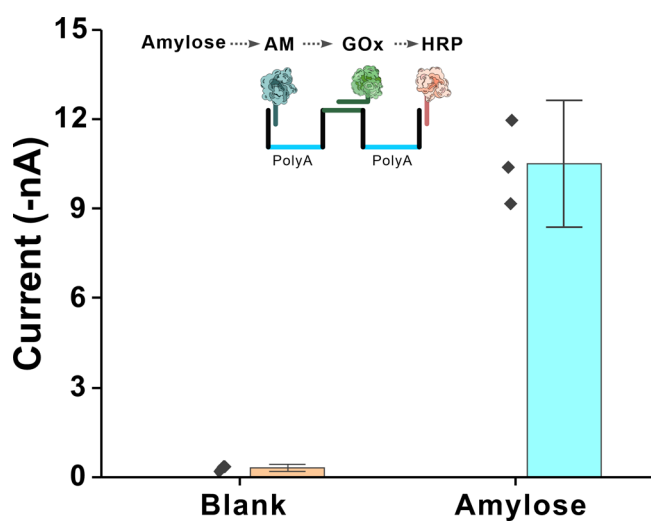


Figure 6. Analysis result of amylose using the trienzyme cascade system of AM/GO_x/HRP. The inset is a schematic illustration of the trienzyme cascade reaction.

spatial regulation of the enzymes on the interface was a critical challenge. In this work, we successfully constructed an enzyme cascade system on a triblock polyA probe (PAP) and realized the electrochemical analysis of glucose. Our approach utilized self-assembled polyA probes to anchor two DNA labeled enzymes (GOx and HRP) onto the electrode surface, forming a high-efficiency one-to-one enzyme cascade. The polyA-based interface not only provided stable and well-arranged self-assembling layers but also allowed for convenient control of the molecular distance between the enzymes. We demonstrated the precise regulation of the molecular distance using the polyA probe, which greatly influenced the catalytic efficiency of the enzyme cascade reaction.

We verified the enzyme cascade reaction and optimized various experimental conditions to achieve the optimal performance of the biosensor. The PAP-based biosensor exhibited excellent detection capability for glucose, with a linear range from 0.05 to 1 mM and a low detection limit of 1.6 μ M. The practicality of the sensor was demonstrated by successful detection of glucose in human serum samples, with recoveries close to 100% and low relative standard deviation.

Furthermore, the biosensor showed excellent specificity for glucose detection compared to other similar sugars.

The generalizability of our enzyme cascade system was proven by constructing a trienzyme cascade reaction, which successfully activated the cascade reaction of AM/GO_x/HRP. This demonstrated the potential scalability of our approach for multienzyme reactions. However, the challenge of long DNA synthesis and surface arrangement of multifragment DNA still need to be solved for further development of the enzyme cascade reaction on multiblock polyA DNA probes.

In summary, our electrochemical biosensor, based on an enzyme cascade reaction, provides a promising platform for the development of point-of-care testing. It offers several advantages, including high sensitivity, easy operation, and high efficiency. Importantly, its versatility can be further extended by the introduction of other enzyme cascade systems.

EXPERIMENTAL SECTION

Materials

DNA oligonucleotides were synthesized and purified by Shanghai BiOligo Biotech (Table 3). Glucose oxidase (*Aspergillus niger*), horseradish peroxidase (Type VI-A), HEPES sodium salt, tris-buffered saline (pH 8.0), tris(2-carboxyethyl) phosphine hydrochloride (TCEP), 2,2'-azino-bis(3-ethylbenzothiazoline-6-sulfonic acid) diammonium salt (ABTS) and dimethyl sulfoxide (DMSO) were purchased from Sigma-Aldrich and used without further purification. SPDP and TMB substrate were purchased from Thermo scientific. ¹³C₆-D-glucose was purchased from Cambridge Isotope Laboratories, Inc. Galactose, fructose, sucrose, xylose, mannose, and glucose were purchased from Sinopharm Chemical Reagent Co. Ltd.

All the buffer solutions were prepared with Milli-Q water from a Millipore system (18.2 M Ω ·cm at 25 $^{\circ}$ C) and stored at 4 $^{\circ}$ C in dark. The immobilization buffer (pH 7.4) contained 10 mM Tris, 1 M NaCl and 1 mM EDTA. The hybridization buffer (pH 7.4) contained 10 mM phosphate buffer and 1 M NaCl. The washing buffer (pH 7.4) contained 10 mM phosphate buffer and 10 mM NaCl. The TBE buffer (pH 8.2) contained 89 mM Tris, 89 mM boric acid, and 10 mM EDTA. The TBS buffer (pH 8.0) contained 50 mM Tris, 138 mM NaCl, and 2.7 mM MgCl.

Table 3. DNA Sequences in This Work

Name	Sequence (5'-3')
PolyA10	TATCATCCTTACACCTCACTAAAAAAAAAACCCCTCTAACTCCATCACA
PolyA 20	TATCATCCTTACACCTCACTAAAAAAAAAAAAAAAAAACCCCTCTAACTCCATCACA
PolyA 30	TATCATCCTTACACCTCACTAAAAAAAAAAAAAAAAAACCCCTCTAACTCCATCACA
PolyA 40	TATCATCCTTACACCTCACTAAAAAAAAAAAAAAAAAACCCCTCTAACTCCATCACA
PolyA 50	TATCATCCTTACACCTCACTAAAAAAAAAAAAAAAAAACCCCTCTAACTCCATCACA
PolyA 60	TATCATCCTTACACCTCACTAAAAAAAAAAAAAAAAAACCCCTCTAACTCCATCACA
PolyA 70	TATCATCCTTACACCTCACTAAAAAAAAAAAAAAAAAACCCCTCTAACTCCATCACA
PolyA 80	TATCATCCTTACACCTCACTAAAAAAAAAAAAAAAAAACCCCTCTAACTCCATCACA
PolyA 90	TATCATCCTTACACCTCACTAAAAAAAAAAAAAAAAAACCCCTCTAACTCCATCACA
PolyA 100	TATCATCCTTACACCTCACTAAAAAAAAAAAAAAAAAACCCCTCTAACTCCATCACA
CP1-SH	TATCATCCTTACACCTCACTTTTTTTTTTT-SH
CP2-SH	SH-TTTTTTTTTTACCCTCTAACTCCATCACA
L1	AGTGAGGTGTAAGGATGATTTTTTTTTT-SH
L2	SH-TTTTTTTTTTGTGATGGAAGTTAGAGGGT
CP1-polyA	TATCATCCTTACACCTCACTAAAAAAAAAACCCCTCTAACTCCATCACA
CP2-polyA	AAAAAAAAAAAAAAAAAACCCCTCTAACTCCATCACA

Preparation of DNA-Tagged Enzyme (DNA-Enzyme)

Two DNA-enzyme complexes were prepared following a previously reported method²¹ with slight modifications. To begin, 100 μL of 40 μM GOx in 50 mM HEPES (pH 7.5) was mixed with 2, 5, 10, or 20-fold SPDP and incubated for 2 h at room temperature in the dark. Excess SPDP was eliminated by passing the reaction mixture through a 30-kD cutoff filter (Amicon). Simultaneously, thiol-modified DNA (L1 for GOx) was freshly prepared by incubating it with a 20-fold excess of TCEP for one h at room temperature in the dark. Excess TCEP was removed using a 3-kD cutoff filter (Amicon). Next, the SPDP-modified enzymes were conjugated to a 10-fold excess of SH-DNA by incubating them together for 2 h at room temperature in the dark. The same procedure was repeated for coupling HRP with L2 DNA. Finally, the excess SH-DNA was washed and filtered using Amicon 30 kD cutoff filters to obtain the desired DNA-enzyme complexes.

Treatment of the Electrode and Construction of the SAM

The surface of a gold electrode (2 mm in diameter) was polished with 0.05 μm alumina particles on microcloth and then sonicated in ethanol and Milli-Q water for 3 min each. Subsequently, the electrodes underwent electrochemically treatment through a series of oxidation and reduction cycling in 0.5 M H_2SO_4 solution. Finally, the electrodes were rinsed with water and dried with nitrogen.

Following the cleaning process, the electrodes were incubated overnight at room temperature in immobilization buffer containing 1 μM triblock polyA capture probe (CP50). The probe-modified electrodes were then treated with 0.1 μM MCH for 30 min at room temperature, followed by thorough rinsing with a washing buffer. Subsequently, the electrodes were incubated for 2 h at 37 $^\circ\text{C}$ in a hybridization buffer containing 0.5 μM GOx-L1 and 0.05 μM HRP-L2. Finally, the electrodes were rinsed again with the washing buffer and subjected to electrochemical measurements.

Electrochemical Measurement

Electrochemical measurements were performed in the TMB substrate using a CHI 630E electrochemical workstation and a conventional three-electrode system, which contains a Ag/AgCl reference electrode, a Pt counter electrode, and a gold working electrode. Cyclic Voltammetry (CV) was carried out at a scan rate of 50 mV/s. Amperometric detection was performed at 100 mV and the electrochemical reduction current was recorded for 100 s after the HRP catalytic reaction reached steady state.

Polyacrylamide Gel Analysis

Polyacrylamide gel electrophoresis was performed with a Bio-Rad mini-protean tetra system. The DNA samples were loaded onto 8% native polyacrylamide gel in the Tris/borate/EDTA (TBE) buffer for 1.5 h at 120 V. After staining by DNA Gel Stain for 30 min, gel images were obtained by Bio-Rad imaging system.

Preparation of AuNP-DNA (AuNP-L1 and AuNP-L2)

The conjugation of AuNPs with sulfhydryl DNA (L1 and L2 separately) was performed mainly based on a previously reported method: "freezing method".²⁶ First, the DNA solution and AuNPs were mixed at a mole ratio of 100/1 and then shaken vigorously for 5 min for thorough mixing. After that the mixture was placed under -20 $^\circ\text{C}$ for 1 h, followed by 3 repeated centrifugation steps at 15 000 rpm for 20 min each, and finally quantified by a UV/vis spectrophotometer. The produced sulfhydryl DNA-modified AuNPs (AuNP-L1 and AuNP-L2) were abbreviated as Au-DNA in this manuscript.

AFM Characterization of the AuNPs on the PAP Covered Surface

To combine AuNP-L1 and AuNP-L2 onto the PAP interface, the following steps were followed: First, PAP was added onto the surface of a gold flake (Au111) and incubated overnight at room temperature for approximately 8 h. Subsequently, it was washed with deionized water and dried by using N_2 . Next, 10 μL of AuNP (consisting of AuNP-L1 and AuNP-L2) was

added onto the PAP-covered gold surface and allowed to incubate for 2 h at room temperature. Finally, the gold flake was characterized using a liquid atomic force microscope (AFM, Bruker, MultiMode 8).

TEM Characterization of the AuNPs on the PAP Covered Surface

To begin with, two conjugations of DNA-AuNP (AuNP-L1 and AuNP-L2) were allowed to react with PAP in a solution for 2 h at room temperature. The resulting incubation product was then deposited onto ultrathin carbon films and left to stand for 10 min. Subsequently, the carbon films underwent three rounds of washing with deionized water, followed by baking under an infrared lamp at 30 °C for 30 min. Finally, all the carbon films were sequentially imaged using field emission transmission electron microscopy (TEM, FEI, TECNAI G2).

■ ASSOCIATED CONTENT

Supporting Information

The Supporting Information is available free of charge at <https://pubs.acs.org/doi/10.1021/jacsau.3c00673>.

Preparation of the DNA-tagged enzyme, characterization of the capability of PAP for the molecule arrangement on the interface, comparison and optimization experiment about the electrochemical assay, and glucose quantification using ID LC-MS/MS and ID GC-MS (PDF)

■ AUTHOR INFORMATION

Corresponding Authors

Shiping Song – *Institute of Materiobiology, Department of Chemistry, College of Science, Shanghai University, Shanghai 200444, China*; orcid.org/0000-0002-0791-8012;

Email: spsong@shu.edu.cn

Gang Liu – *Key Laboratory of Bioanalysis and Metrology for state market regulation, Shanghai Institute of Measurement and Testing Technology, Shanghai 201203, China*;

orcid.org/0000-0003-3779-7212; Email: liug@simt.com.cn

Yanli Wen – *Key Laboratory of Bioanalysis and Metrology for state market regulation, Shanghai Institute of Measurement and Testing Technology, Shanghai 201203, China*;

Email: wenyl@simt.com.cn

Authors

Lele Wang – *Key Laboratory of Bioanalysis and Metrology for state market regulation, Shanghai Institute of Measurement and Testing Technology, Shanghai 201203, China*

Ruiyan Guo – *Key Laboratory of Bioanalysis and Metrology for state market regulation, Shanghai Institute of Measurement and Testing Technology, Shanghai 201203, China*

Lanying Li – *Key Laboratory of Bioanalysis and Metrology for state market regulation, Shanghai Institute of Measurement and Testing Technology, Shanghai 201203, China*

Qing Tao – *Key Laboratory of Bioanalysis and Metrology for state market regulation, Shanghai Institute of Measurement and Testing Technology, Shanghai 201203, China*

Qin Xu – *Key Laboratory of Bioanalysis and Metrology for state market regulation, Shanghai Institute of Measurement and Testing Technology, Shanghai 201203, China*

Xue Yang – *Key Laboratory of Bioanalysis and Metrology for state market regulation, Shanghai Institute of Measurement and Testing Technology, Shanghai 201203, China*

Xue Liu – *Institute of Materiobiology, Department of Chemistry, College of Science, Shanghai University, Shanghai 200444, China*

Jiang Li – *Institute of Materiobiology, Department of Chemistry, College of Science, Shanghai University, Shanghai 200444, China*

Lihua Wang – *Institute of Materiobiology, Department of Chemistry, College of Science, Shanghai University, Shanghai 200444, China*

Jinxue Chang – *Key Laboratory of Bioanalysis and Metrology for state market regulation, Shanghai Institute of Measurement and Testing Technology, Shanghai 201203, China*

Chengming Cao – *Key Laboratory of Bioanalysis and Metrology for state market regulation, Shanghai Institute of Measurement and Testing Technology, Shanghai 201203, China*

Complete contact information is available at: <https://pubs.acs.org/10.1021/jacsau.3c00673>

Author Contributions

[†]L.W. and R.G. contributed equally to this work. L.W. and Q.T. performed the electrochemical analysis. R.G. and X.Y. conducted AFM experiments. L.L. and J.C. provided TEM characterization. Q.X. conducted LC-MS/MS and GC-MS experiments. C.C. and Y.W. contributed to the writing and editing of the manuscript. X.L., J.L., and L.W. provided input and guidance throughout the research process. S.S. and G.L. supervised the project. All authors reviewed and approved the final version of the manuscript.

Funding

This work was financially supported by The National Quality Infrastructure Program of China (2021YFF0600901 NQI), Shanghai Sailing Program (21YF1459500), The National Natural Science Foundation of China (No. 22074093, 21974147), and the Natural Science Foundation of Shanghai Municipal (Nos. 20ZR1424100).

Notes

The authors declare no competing financial interest.

■ REFERENCES

- (1) Agapakis, C. M.; Boyle, P. M.; Silver, P. A. Natural strategies for the spatial optimization of metabolism in synthetic biology. *Nat. Chem. Biol.* **2012**, *8* (6), 527–535.
- (2) Savage, D. F.; Afonso, B.; Chen, A. H.; Silver, P. A. Spatially Ordered Dynamics of the Bacterial Carbon Fixation Machinery. *Science* **2010**, *327* (5970), 1258–1261.
- (3) Rabe, K. S.; Muller, J.; Skoupi, M.; Niemeyer, C. M. Cascades in Compartments: En Route to Machine-Assisted Biotechnology. *Angew. Chem., Int. Ed. Engl.* **2017**, *56* (44), 13574–13589.
- (4) Dueber, J. E.; Wu, G. C.; Malmirchegini, G. R.; Moon, T. S.; Petzold, C. J.; Ullal, A. V.; Prather, K. L.; Keasling, J. D. Synthetic protein scaffolds provide modular control over metabolic flux. *Nat. Biotechnol.* **2009**, *27* (8), 753–759.
- (5) Wang, C.; Yue, L.; Willner, I. Controlling biocatalytic cascades with enzyme-DNA dynamic networks. *Nat. Catal.* **2020**, *3* (11), 941–950.
- (6) Wang, H.; Zhao, Z.; Liu, Y.; Shao, C.; Bian, F.; Zhao, Y. Biomimetic enzyme cascade reaction system in microfluidic electro-spray microcapsules. *Sci. Adv.* **2018**, *4* (6), No. eaat2816.

- (7) Benítez-Mateos, A. I.; Roura Padrosa, D.; Paradisi, F. Multistep enzyme cascades as a route towards green and sustainable pharmaceutical syntheses. *Nat. Chem.* **2022**, *14* (5), 489–499.
- (8) Mohammad, M.; Razmjou, A.; Liang, K.; Asadnia, M.; Chen, V. Metal-Organic-Framework-Based Enzymatic Microfluidic Biosensor via Surface Patterning and Biomineralization. *ACS Appl. Mater. Interfaces* **2019**, *11* (2), 1807–1820.
- (9) Lin, J.-L.; Wheeldon, I. Kinetic Enhancements in DNA-Enzyme Nanostructures Mimic the Sabatier Principle. *ACS Catal.* **2013**, *3* (4), 560–564.
- (10) Liang, J.; Mazur, F.; Tang, C.; Ning, X.; Chandrawati, R.; Liang, K. Peptide-induced super-assembly of biocatalytic metal-organic frameworks for programmed enzyme cascades. *Chem. Sci.* **2019**, *10* (34), 7852–7858.
- (11) Chen, W.-H.; Vázquez-González, M.; Zoabi, A.; Abu-Reziq, R.; Willner, I. Biocatalytic cascades driven by enzymes encapsulated in metal-organic framework nanoparticles. *Nat. Catal.* **2018**, *1* (9), 689–695.
- (12) Liu, C.; Xing, J.; Akakuru, O. U.; Luo, L.; Sun, S.; Zou, R.; Yu, Z.; Fang, Q.; Wu, A. Nanozymes-Engineered Metal-Organic Frameworks for Catalytic Cascades-Enhanced Synergistic Cancer Therapy. *Nano Lett.* **2019**, *19* (8), 5674–5682.
- (13) Wilner, O. I.; Weizmann, Y.; Gill, R.; Lioubashevski, O.; Freeman, R.; Willner, I. Enzyme cascades activated on topologically programmed DNA scaffolds. *Nat. Nanotechnol.* **2009**, *4* (4), 249–254.
- (14) Jones, M. R.; Seeman, N. C.; Mirkin, C. A. Nanomaterials. Programmable materials and the nature of the DNA bond. *Science* **2015**, *347* (6224), 1260901–1260901.
- (15) Pinheiro, A. V.; Han, D.; Shih, W. M.; Yan, H. Challenges and opportunities for structural DNA nanotechnology. *Nat. Nanotechnol.* **2011**, *6* (12), 763–772.
- (16) Liu, M.; Fu, J.; Hejesen, C.; Yang, Y.; Woodbury, N. W.; Gothelf, K.; Liu, Y.; Yan, H. A DNA tweezer-actuated enzyme nanoreactor. *Nat. Commun.* **2013**, *4* (1), 2127–2127.
- (17) Yin, F. F.; Zhao, H. P.; Lu, S. S.; Shen, J. W.; Li, M.; Mao, X. H.; Li, F.; Shi, J. Y.; Li, J.; Dong, B. J.; Xue, W.; Zuo, X. L.; Yang, X. R.; Fan, C. H. DNA-framework-based multidimensional molecular classifiers for cancer diagnosis. *Nat. Nanotechnol.* **2023**, *18* (6), 677–686.
- (18) Hu, Q.; Li, H.; Wang, L.; Gu, H.; Fan, C. DNA Nanotechnology-Enabled Drug Delivery Systems. *Chem. Rev.* **2019**, *119* (10), 6459–6506.
- (19) Fu, J.; Yang, Y. R.; Johnson-Buck, A.; Liu, M.; Liu, Y.; Walter, N. G.; Woodbury, N. W.; Yan, H. Multi-enzyme complexes on DNA scaffolds capable of substrate channelling with an artificial swinging arm. *Nat. Nanotechnol.* **2014**, *9* (7), 531–536.
- (20) Zhao, Z.; Fu, J.; Dhakal, S.; Johnson-Buck, A.; Liu, M.; Zhang, T.; Woodbury, N. W.; Liu, Y.; Walter, N. G.; Yan, H. Nanocaged enzymes with enhanced catalytic activity and increased stability against protease digestion. *Nat. Commun.* **2016**, *7*, 10619–10619.
- (21) Fu, J.; Yang, Y. R.; Dhakal, S.; Zhao, Z.; Liu, M.; Zhang, T.; Walter, N. G.; Yan, H. Assembly of multienzyme complexes on DNA nanostructures. *Nat. Protoc.* **2016**, *11* (11), 2243–2273.
- (22) Fu, J.; Liu, M.; Liu, Y.; Woodbury, N. W.; Yan, H. Interenzyme substrate diffusion for an enzyme cascade organized on spatially addressable DNA nanostructures. *J. Am. Chem. Soc.* **2012**, *134* (12), 5516–5519.
- (23) Song, P.; Shen, J.; Ye, D.; Dong, B.; Wang, F.; Pei, H.; Wang, J.; Shi, J.; Wang, L.; Xue, W.; Huang, Y.; Huang, G.; Zuo, X.; Fan, C. Programming bulk enzyme heterojunctions for biosensor development with tetrahedral DNA framework. *Nat. Commun.* **2020**, *11* (1), 838–838.
- (24) Browne, W. R.; Feringa, B. L. Making molecular machines work. *Nat. Nanotechnol.* **2006**, *1* (1), 25–35.
- (25) Li, L.; Wang, L.; Xu, Q.; Xu, L.; Liang, W.; Li, Y.; Ding, M.; Aldalbah, A.; Ge, Z.; Wang, L.; Yan, J.; Lu, N.; Li, J.; Wen, Y.; Liu, G. Bacterial Analysis Using an Electrochemical DNA Biosensor with Poly-Adenine-Mediated DNA Self-Assembly. *ACS Appl. Mater. Interfaces* **2018**, *10* (8), 6895–6903.
- (26) Lu, C.; Liu, X.; Li, Y.; Yu, F.; Tang, L.; Hu, Y.; Ying, Y. Multifunctional Janus hematite-silica nanoparticles: mimicking peroxidase-like activity and sensitive colorimetric detection of glucose. *ACS Appl. Mater. Interfaces* **2015**, *7* (28), 15395–15402.
- (27) Sun, R.; Lv, R.; Zhang, Y.; Du, T.; Li, Y.; Chen, L.; Qi, Y. Colorimetric sensing of glucose and GSH using core-shell Cu/Au nanoparticles with peroxidase mimicking activity. *RSC Adv.* **2022**, *12* (34), 21875–21884.
- (28) Li, M.; Liu, C.; Qi, L.; Liu, H. Nitrogen-Doped Graphene Quantum Dots Anchored on Hollow Zeolitic Imidazolate Framework-8 Colloidosomes for Fluorescence Detection of Glucose. *ACS Appl. Nano Mater.* **2022**, *5* (4), 5425–5438.
- (29) Niu, X.; Gao, H.; Du, J. CsPbBr₃ Perovskite Nanocrystals Decorated with Cu Nanoclusters for Ratiometric Detection of Glucose. *ACS Appl. Nano Mater.* **2022**, *5* (2), 2350–2357.
- (30) Wang, Z.; Guo, H.; Luo, Z.; Duan, Y.; Feng, Y. Low-Triggering-Potential Electrochemiluminescence from a Luminol Analogue Functionalized Semiconducting Polymer Dots for Imaging Detection of Blood Glucose. *Anal. Chem.* **2022**, *94* (14), 5615–5623.
- (31) Myndrul, V.; Coy, E.; Babayevska, N.; Zahorodna, V.; Balitskyi, V.; Baginskiy, I.; Gogotsi, O.; Bechelany, M.; Giardi, M. T.; Iatsunskyi, I. MXene nanoflakes decorating ZnO tetrapods for enhanced performance of skin-attachable stretchable enzymatic electrochemical glucose sensor. *Biosens Bioelectron.* **2022**, *207*, 114141–114141.
- (32) Barbee, B.; Muchharla, B.; Adedeji, A.; Karoui, A.; Kumar Sadasivuni, K.; Sha, M. S.; Abdullah, A. M.; Slaughter, G.; Kumar, B. Cu and Ni Co-sputtered heteroatomic thin film for enhanced nonenzymatic glucose detection. *Sci. Rep.* **2022**, *12* (1), 7507–7507.